Russian Journal of Earth Sciences Online ISSN: 1681-1208

Investigation of L-Band Radar Signal Scattering From Ice Cover Using GNSS-R Data

Dmitry Kovaldov*[,1], Vladimir Karaev[1], Yuriy Titchenko[1], Vyacheslav Fateev[2], Vladislav Lopatin[2], Feixiong Huang[3], Xiaoli Wang[4], and Jie Guo[4]

[1]Institute of Applied Physics, Russian Academy of Sciences, Nizhny Novgorod, Russian Federation
[2]Russian Metrological Institute of Technical Physics and Radioengineering, Solnechnogorsk, Russian Federation
[3]National Space Science Center, Chinese Academy of Sciences, Beijing, China
[4]Yantai Institute of Coastal Zone Research, Chinese Academy of Sciences, Yantai, China
* **Correspondence to:** Dmitry Kovaldov, dmit.kovaldov@gmail.com

Abstract: Freshwater ice cover on inland water bodies is a sensitive indicator of climate change, and its monitoring is hampered by the decline of in situ observation networks since the 1980s. Previous applications of GNSS-Reflectometry (GNSS-R) have focused mainly on sea ice detection, while its capability for seasonal freshwater ice monitoring has remained insufficiently explored. The aim of this study is to assess the sensitivity of spaceborne L-band bistatic measurements to the processes of freshwater ice cover formation, growth, and break-up on large inland lakes, and to compare the scattering behavior with that of sea ice. A full annual cycle (September 2023 – August 2024) was analyzed using data from the GNOS-II instrument onboard the Feng-Yun 3E (FY-3E) satellite at two test sites: Great Slave Lake (Canada) for freshwater ice and the Sea of Okhotsk for sea ice. Statistical moments of the Doppler spectrum – width and kurtosis coefficient – were computed from delay-Doppler maps. The results were validated against meteorological records from the Yellowknife station, MODIS imagery, and ERA5 ice thickness reanalysis. A monotonic decrease in Doppler spectrum width with decreasing air temperature was established for freshwater ice, consistent with a reduction of effective surface roughness. For freshwater ice, peak power and kurtosis coefficient show a distinct dependence on ice thickness, reflecting signal attenuation within the ice volume and dominant reflection at the ice-water interface; for sea ice these parameters remain stable, since reflection occurs at the air-ice boundary owing to high brine salinity. The findings demonstrate that L-band bistatic reflectometry provides an effective all-weather tool for operational monitoring of freshwater and sea ice, including detection of freeze-up and break-up phases, ice thickness estimation, and support for Arctic navigation.

Keywords: Bistatic scheme, Doppler spectrum, delay-Doppler map, freshwater ice, sea ice, Great Slave Lake, Sea of Okhotsk, FY-3E satellite, kurtosis coefficient, ice thickness

Citation: Kovaldov D., Karaev V., Titchenko Y., Fateev V., Lopatin V., Huang F., Wang X., and Guo J. (2026), Investigation of L-Band Radar Signal Scattering From Ice Cover Using GNSS-R Data, *Russian Journal of Earth Sciences*, 26, ES1020, EDN: DTFEFT, https://doi.org/10.2205/2026es001133

Research Article

Received: February 25, 2026
Accepted: April 21, 2026
Published: April 27, 2026

1. Introduction

Freshwater ice cover, which forms during the winter season on inland water bodies (rivers, lakes, etc.), along with sea ice, constitutes an important component of the global cryosphere. Investigating the dynamic changes in ice cover parameters of inland freshwater water bodies is essential for understanding and predicting future climate change [*Brown and Duguay*, 2010; *Duguay et al.*, 2014]. Lakes cover approximately 2% of the Earth's surface. They are primarily concentrated in the Northern Hemisphere and tundra regions, where they cover 15 to 40% of the land area. Such ice-covered areas play a significant role in the climatic processes of these regions [*Duguay et al.*, 2014; *Lehner and Doll*, 2004]. In addition to lake ice, river ice also affects the hydrological system, as it impacts 58% of the total

river length in the Northern Hemisphere [*Prowse et al.*, 2007]. The presence of ice cover influences the biological, chemical, and physical processes in water bodies of cold regions. Lake ice variability is used as a sensitive indicator of climate change [*Brown and Duguay*, 2010; *Duguay et al.*, 2014; *Sharma et al.*, 2021]. Observations of freeze-up/break-up timing of ice cover are important, as projected global warming, particularly at northern latitudes, will lead to significant changes that may increase the influence of lakes on regional energy and water balance [*Duguay et al.*, 2014; *Long et al.*, 2007]. Beyond environmental factors, ice cover has important socio-economic implications [*Duguay et al.*, 2014; *Prowse et al.*, 2007], affecting hydroelectric power generation and transportation routes (the duration of ice road use or river navigation). Ice jams on rivers can cause damage to infrastructure and lead to flooding [*Duguay et al.*, 2014; *Prowse et al.*, 2007]. Accurate representation of lake ice in numerical models is an important step toward improving global climate models and forecasting extreme weather events [*Long et al.*, 2007; *Sharma et al.*, 2021].

Since the 1980s, a decline in ground-based observations has been observed, which has led to an increasing role of satellite remote sensing [*Latifovic and Pouliot*, 2007]. Various remote sensing methods are employed for freshwater ice monitoring, for example, those utilizing optical data, as well as radar measurements performed by a variety of instruments, such as scatterometers, radiometers, radar altimeters, and synthetic aperture radars (SAR) [*Duguay et al.*, 2014].

Optical methods are based on semi-automated image interpretation [*Hall et al.*, 2002; *Latifovic and Pouliot*, 2007]. Satellite radiometer data in the infrared (IR) and microwave ranges are also widely used for tracking ice cover freeze-up and break-up processes. In particular, threshold algorithms based on reflectance values have been applied when working with historical AVHRR data at a spatial resolution of 1.1 km [*Hall et al.*, 1994; *Latifovic and Pouliot*, 2007]. MODIS products with a resolution of 500 m are also used for determining freshwater ice cover parameters [*Hall et al.*, 2002; *Kropáček et al.*, 2013]. However, the applicability of optical and infrared (IR) data is limited by the influence of weather conditions, such as the presence of cloud cover, which is common during the ice formation and break-up seasons, as well as low-light or darkness conditions at high latitudes during the autumn–winter period, which hinders the application of automated algorithms.

Passive microwave radiometry uses brightness temperature values to investigate processes occurring within the ice cover [*Kang et al.*, 2010]. Compared to IR remote sensing methods, microwave radiometry allows data acquisition regardless of cloud cover, which is particularly important for polar and subpolar regions. However, its main disadvantage is low spatial resolution. In studies of large northern lakes – Great Bear Lake and Great Slave Lake – it was shown that the AMSR-E channel at 18.7 GHz with horizontal polarization is most suitable for tracking freeze-up/break-up processes [*Kang et al.*, 2010, 2014]. Furthermore, analysis of the temporal evolution of brightness temperature in the 10.7 GHz and 18.7 GHz AMSR-E channels during the ice growth period demonstrated a strong correlation with ice thickness estimated using a numerical model [*Kang et al.*, 2010]. This approach enabled the development of regression algorithms for monthly ice thickness estimation on Great Bear Lake and Great Slave Lake [*Kang et al.*, 2014].

Active microwave remote sensing (SAR and scatterometry) is widely used owing to its independence from cloud cover and illumination conditions. Ku-band scatterometers, such as SeaWinds, have been used for mapping the spatial distribution of ice cover parameters on Great Bear Lake and Great Slave Lake, as the onset of freeze-up and break-up is associated with observed changes in the backscattering cross-section [*Howell et al.*, 2009]. SAR is the preferred instrument for river ice type classification, as it offers significantly better spatial resolution (several meters) and the reflected signal is sensitive to surface roughness and ice texture, particularly to air bubbles [*Gherboudj et al.*, 2010; *Weber et al.*, 2003]. C-band SAR enables differentiation of ice types on rivers, and the use of multiple polarizations can improve classification accuracy [*Leigh et al.*, 2014; *Mermoz et al.*, 2014; *Weber et al.*, 2003]. SAR data, owing to the ability of microwave signals to penetrate freshwater ice under dry

snow conditions (positive air temperature), are useful for obtaining information about the internal structure of ice [*Duguay et al.*, 2002; *Jeffries et al.*, 1994; *Mätzler and Wegmüller*, 1987]. In shallow Arctic and subarctic lakes, SAR images can be used for monitoring the seasonal evolution of floating and grounded ice, as floating ice containing bubbles exhibits higher backscatter than grounded ice, with a sharp and significant signal change visible when the water body freezes completely to the bottom [*Duguay and Lafleur*, 2003; *Duguay et al.*, 2002; *Jeffries et al.*, 1994].

Radar altimeters are also used for monitoring the ice regime of large inland water bodies. For example, on large lakes such as Baikal, Ladoga, and Onega, radar altimeter and passive microwave radiometry data are used to discriminate between ice and water surface types. For lakes covered with seasonal ice, ice cover parameters are determined from the shape of the received pulse (characteristic extrema are present on the leading edge of the reflected pulse), which is formed by reflections from multiple medium layers (air/snow, snow/ice, ice/water) [*Kouraev et al.*, 2007]. For large rivers, such as the Ob, a methodology based on radar altimeter data enables surface type discrimination with good agreement with ground-based observations [*Yang et al.*, 2021].

A novel approach to freshwater ice cover monitoring is the use of radars operating at low incidence angles ($\theta < 12°$) [*Karaev et al.*, 2018; *Panfilova and Karaev*, 2024]. The Dual-frequency Precipitation Radar (DPR), installed on the GPM satellite, performs measurements in the Ku- and Ka-bands, covering most inland water bodies of Russia and Canada owing to its orbital inclination of 65°. At low incidence angles, the backscattering cross-section of the water surface is significantly higher than that of land [*Panfilova and Karaev*, 2023]. This allows the detection of water bodies (e.g., rivers 400–500 m wide) that are smaller than the DPR resolution cell (5 km) [*Karaev et al.*, 2025]. It was shown that "water-to-ice" and "ice-to-water" transitions can be detected through the analysis of DPR radar data, as after ice formation the river becomes "invisible" in the radar image [*Panfilova and Karaev*, 2023]. The problem of sea ice detection by an orbital microwave Doppler radar at nadir sensing was also addressed in [*Karaev et al.*, 2022]. The DPR possesses a multi-year data archive, which is an important advantage for assessing climate change trends.

In recent decades, there has been a clear trend toward the reduction of ground-based observation networks (gauging stations) for freshwater ice. For instance, in Canada, the network of stations monitoring lake freeze-up and break-up dates, which had comprised 757 sites, decreased to approximately 10% of the 1984–1985 level by 1997–1998 due to large-scale budget cuts in government agencies. In particular, regular ground-based measurements of ice cover thickness on Great Slave Lake near the city of Yellowknife, conducted by Environment and Climate Change Canada (ECCC) since 1958, were discontinued after 2016. In this context, research continues to be directed toward the development of new effective remote sensing technologies. One of the promising directions is the use of GNSS-Reflectometry (GNSS-R) methods [*Yan and Huang*, 2016]. This method is based on the use of GNSS signals reflected from the Earth's surface. In addition to ice cover investigation, GNSS signals reflected from the water surface are also applied in geodetic tasks, in particular for determining the geoid height profile and vertical deflection [*Lopatin et al.*, 2024]. Measurements using this method are performed in the L-band, which is insensitive to weather conditions. A distinctive feature of the GNSS-R method is its bistatic sensing geometry. In a monostatic sensing configuration, the backscattered signal is received (as in DPR), whereas in the bistatic configuration, the forward-scattered signal is received; however, the mechanism remains quasi-specular, similar to remote sensing at low incidence angles with monostatic radars.

Previously, these assumptions were used to compare data from the TechDemoSat-1 satellite (TDS-1, 2014–2018) during measurements at a test site in the Sea of Okhotsk with DPR satellite data [*Kovaldov et al.*, 2025]. Numerical simulation of radar signals reflected by the sea surface with varying sea ice concentration further supports the significance of this research direction [*Titchenko et al.*, 2025].

The aim of the present study is to investigate the sensitivity of spaceborne GNSS-R measurements to the processes of freshwater ice cover formation, growth, and break-up on large inland water bodies. Unlike previous GNSS-R studies, which have focused primarily on sea ice detection [*Kovaldov et al.*, 2025; *Titchenko et al.*, 2025], this work applies the method for the first time to seasonal freshwater ice, using data from the GNOS-II instrument onboard the Feng-Yun 3E satellite (FY-3E, 2021–present). A full annual cycle (September 2023 – August 2024) was analyzed at a test site on Great Slave Lake, covering the complete freeze-up and break-up sequence. The GNSS-R observations were compared with meteorological data from the Yellowknife station, MODIS imagery, and ERA5 ice thickness reanalysis, which allowed us to assess the potential of L-band bistatic reflectometry as a tool for freshwater ice monitoring – a capability not previously demonstrated. The characteristics of the GNOS-II instrument and its remote sensing capabilities were described in [*Huang et al.*, 2022].

2. Materials and Methods

This study considers a bistatic remote sensing configuration in which GPS satellites at an orbital altitude of 20,180 km serve as the L1 signal transmitter (1575.42 MHz), and the FY-3E satellite at an orbital altitude of approximately 650 km serves as the receiver. Due to the large difference in orbital altitudes between the transmitter and receiver, the incident wave at the reflecting surface has a constant grazing angle within the illumination footprint (plane wavefront), which determines the specific features of the measurement geometry and the ray paths reaching the receiver after reflection from the surface. The remote sensing configuration is shown in Figure 1.

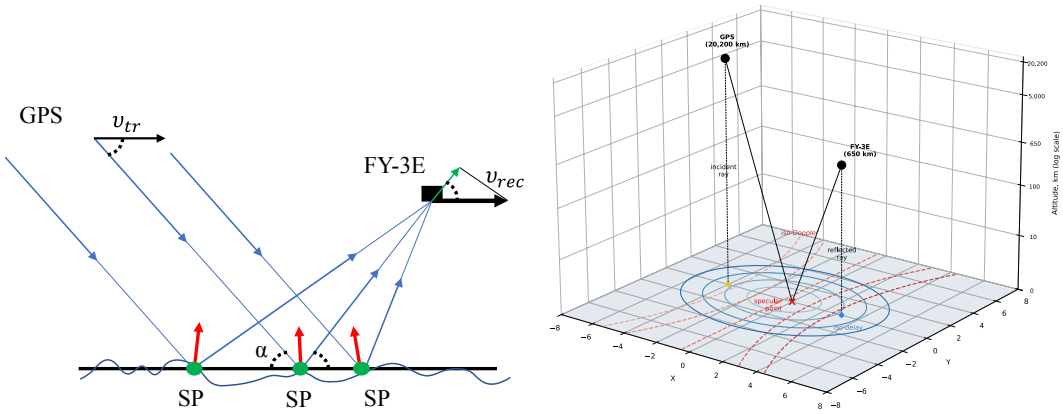

Figure 1. (a) Simplified geometry of bistatic (example of the FY-3E satellite) remote sensing schemes. (b) 3D bistatic sensing scheme with iso-delay (blue lines) and iso-Doppler (red lines) contours.

The reflected signal arrives at the receiver at different reflection/reception angles, each of which has its own Doppler frequency shift, thus forming a Doppler spectrum. One of the primary analysis products in this remote sensing method is the Delay-Doppler Map (DDM), obtained through Fourier transformation and cross-correlation with a model navigation satellite signal. In such a map, each pixel value is the result of applying the Fourier transform and correlation between the GNSS signal received after reflection from the Earth's surface and the GNSS signal generated onboard the satellite. The appearance of such Delay-Doppler maps for signals reflected from different surface types (ice and water) differs significantly in their statistical parameters. Such differences enable the use of raw DDMs for reflecting surface classification in current research. To solve this task, neural networks are applied [*Yan and Huang*, 2018; *Yan et al.*, 2017], or differential characteristics of the DDM maps themselves are analyzed [*Zhu et al.*, 2017]. Here, we will not delve into power calibration issues and will consider statistical moments of the Doppler spectrum.

In this study, the Doppler spectrum (DS) of the reflected signal is analyzed. To obtain the DS, noise, calculated as the average over the first 5 delay values (https://merrbys.co.uk/), is first subtracted from the entire DDM. Then, integration over delay is performed to retain only the dependence on Doppler shift frequencies.

It should be noted that as the signal passes through the ionosphere and troposphere, various effects arise that influence the signal phase and amplitude, including the Faraday effect and ionospheric irregularities. However, the proposed method, based on integration over delays and Doppler spectrum formation, eliminates the influence of phase shift during microwave signal propagation through the ionosphere, since the frequency distribution of Doppler shifts depends only on the projection of the receiver velocity onto the direction of the reflected radiation. Amplitude effects associated with the constantly changing geometry for each specular point can also be disregarded at this stage of the research, as the study is focused on the central statistical moments of the DS, which is an advantage of this data analysis approach.

3. Results and Discussion

Great Slave Lake (Canada) was selected as the test site for investigating the influence of temperature conditions on L-band signal scattering from freshwater ice cover. Data from the FY-3E satellite for the period from September 2023 to August 2024 are considered.

The boundaries of the study area were defined manually, after which specular reflection points falling within this area were selected to exclude the influence of the coastline. The test site and specular reflection points are presented in Figure 2. After applying filtering and noise analysis, 1,970 points were obtained for analysis, corresponding to 169 tracks on different days during the period from September 2023 to August 2024.

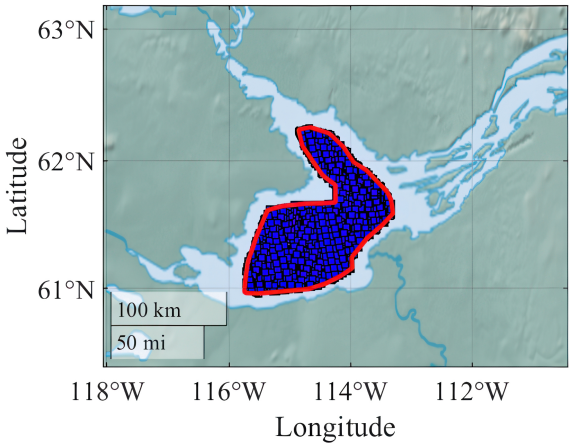

Figure 2. The red line indicates the test site boundaries; squares represent specular reflection points on the surface.

Figure 3 presents visible-range images acquired by the MODIS spectroradiometer onboard the Aqua satellite. Analysis of a series of satellite images allows tracking the dynamics of ice cover formation on the lake surface and establishing that complete freeze-up of the lake occurred in early January.

For additional validation of remote sensing results and confirmation of the timing of stable ice cover establishment, Figure 4 presents data from the meteorological station located in Yellowknife. The meteorological data include air temperature time series, which allow tracking the temperature regime during the freeze-up period and comparing it with satellite observation data. Based on MODIS imagery, it was determined that the first ice appeared on December 5, 2023, and the lake froze completely on January 4, 2024. The ice melted completely by June 4, 2024, with the first open water areas (polynyas) appearing as early as May 16, 2024. The temperature graph shows that positive temperatures began

around April 9, 2024. Thus, in the subsequent analysis of dependencies, we will focus on five intervals: from September 2023 to December 5, 2023 – the open water period; from December 5, 2023 to January 4, 2024 – the ice cover formation process; from January 4, 2024 to April 9, 2024 – the dry ice cover period; from April 9, 2024 to June 4, 2024 – the melting process; and from June 4, 2024 to August 2024 – the open water period.

Figure 3. Images of the test site from MODIS data onboard the Aqua satellite.

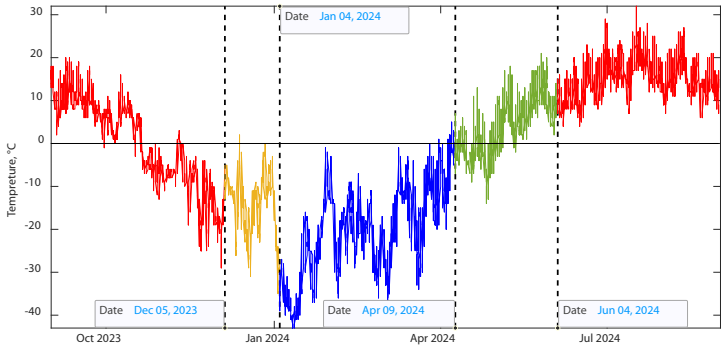

Figure 4. Temperature graph for the region based on meteorological station data from Yellowknife; dashed lines indicate the moments of first ice appearance (December 5, 2023), complete ice cover formation (January 4, 2024), formation of the first polynyas (April 9, 2024), and complete ice cover melting (June 4, 2024).

For all experimental points, DDMs were examined and DSs were calculated. For quantitative analysis of the obtained mean DSs, statistical parameters were selected that characterize the shape of the distribution and are invariant with respect to the absolute signal level, namely: the width

$$\Delta F = 2\sqrt{\frac{\int_{-\infty}^{+\infty}\left(f-\overline{f}\right)^2 S(f)df}{\int_{-\infty}^{+\infty} S(f)df}}, \tag{1}$$

where $S(f)$ is the Doppler spectrum, $\overline{f} = \frac{\int fS(f)df}{\int S(f)df}$ is the first raw moment or the center of mass of the Doppler spectrum, f is the frequency. And the kurtosis coefficient, which characterizes the peakedness of the distribution:

$$\gamma_2 = \frac{\mu_4}{\sigma^4} - 3 = \frac{\int_{-\infty}^{+\infty}\left(f-\overline{f}\right)^4 S(f)df}{\int_{-\infty}^{+\infty} S(f)df} \Big/ \left(\frac{\Delta F}{2}\right)^4 - 3,$$

where μ_4 is the fourth central moment, σ is the standard deviation. Additionally, ERA5 reanalysis data on lake ice cover thickness were used to analyze the influence of thickness on

the DS statistical parameters. Examples of DSs for signals reflected from a wind-roughened water surface and ice cover, with DS width indicated in accordance with the definition given by formula (1), are presented in Figure 5.

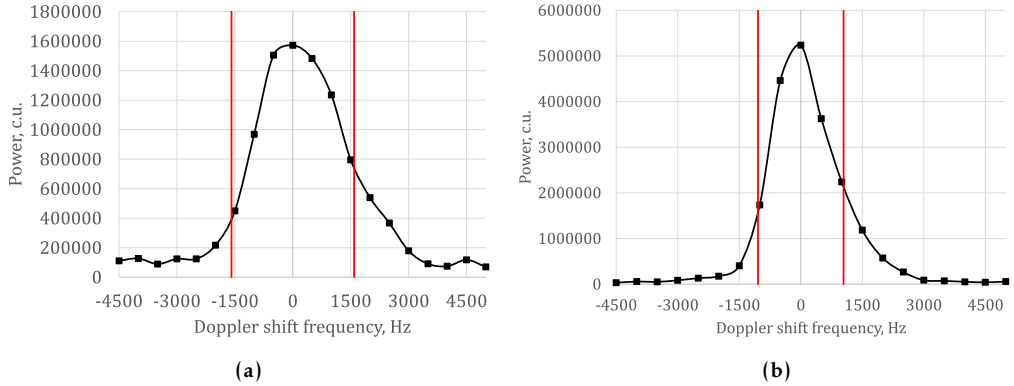

Figure 5. Examples of DSs for water on October 2, 2023 (a) and for ice cover on March 14, 2024 (b). Red lines indicate the determined width: water – 3175 Hz, ice – 2086 Hz.

The dependencies of ice cover thickness from the reanalysis, reflected signal maxima, and calculated statistical moments for all DSs as a function of date are presented in Figure 6. The coordinate system for the reanalysis data is fixed, while the specular reflection points are random in nature; therefore, the ice cover thickness was determined based on the shortest distance between the reanalysis grid nodes and the specular reflection point.

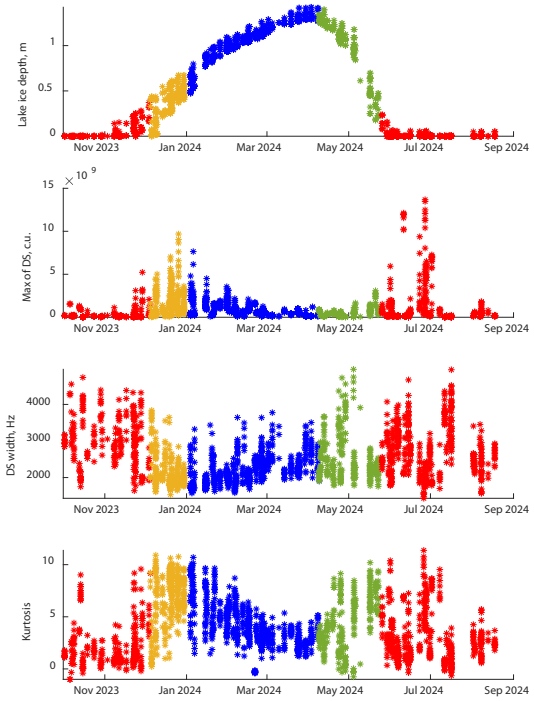

Figure 6. From top to bottom: dependence of ice cover thickness at specular points based on ERA5 reanalysis data, dependence of DS maximum value, dependence of DS width, and dependence of kurtosis on the recording date. Red points indicate measurements made under open water conditions, orange points – after the appearance of first ice, blue points – records under complete freeze-up and sustained negative air temperature, and green points – during air warming and the onset of ice cover melting.

From Figure 6, it can be seen that the freshwater ice cover affects the statistical characteristics of the reflected signal DS. First, it is evident that during the lake freeze-up process, the maximum value initially increases, the width value decreases, and consequently the kurtosis value increases; however, as the ice cover grows thicker, the maximum values begin to decrease, leading to a reduction in kurtosis.

This behavior is related to the fact that the primary signal reflection occurs at the ice–water interface, unlike in the case of sea ice. The signal is attenuated/weakened within the ice cover layer. Subsequently, in April–May, when the lake ice cover begins to melt, the peak power starts to increase again due to the decreasing thickness and the presence of water on the ice cover surface. The ice surface covered with water becomes a good reflector.

Next, let us consider the dependence of statistical parameters on ice cover thickness. For this purpose, block averaging was applied to the obtained dependencies, whereby the data series is thinned and the new values correspond to the mean value of the selected block. In this case, averaging over blocks of 50 points is considered. The dependence of the averaged parameters on date and thickness is presented in Figure 7.

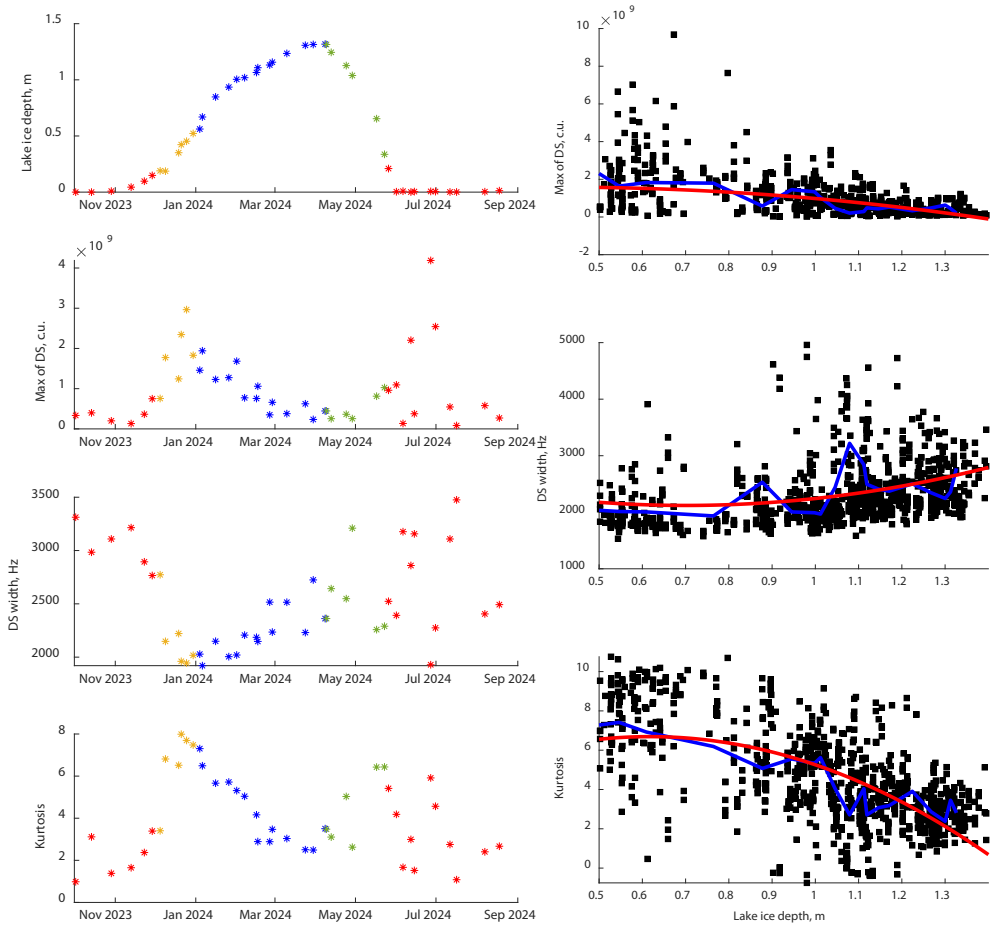

Figure 7. (a) Averaged parameter dependencies on date, where blue indicates a completely frozen lake and sustained negative air temperature, red – open water, orange – after the appearance of first ice, and green – positive air temperature and the onset of polynya formation. (b) Dependence of DS statistical characteristics on ice cover thickness. The blue curve represents the averaged data, and the red curve – polynomial approximation.

For a comparative analysis of the influence of ice cover formation/break-up on the reflected radar signal, the Sea of Okhotsk water area was selected, where analogous statistical parameters were examined for the same period. The spatial boundaries of the study area (red line) and the distribution of specular reflection points (blue squares) within the test site are presented in Figure 8. The study area is a rectangular test site located in the Sea of Okhotsk water area and adjacent regions between the mainland coast of Khabarovsk Krai and the northern part of Sakhalin Island. The test site is bounded by coordinates 54.9–56.2° N and 139.5–141.7° E.

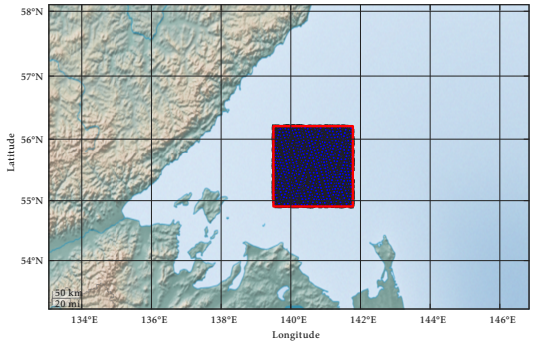

Figure 8. The red line indicates the test site boundaries; squares represent specular reflection points on the surface.

For monitoring ice conditions and determining the timing of stable ice cover formation, Figure 9 presents images acquired by the MODIS spectroradiometer, which allow tracking the spatiotemporal dynamics of ice formation in the study area of the Sea of Okhotsk.

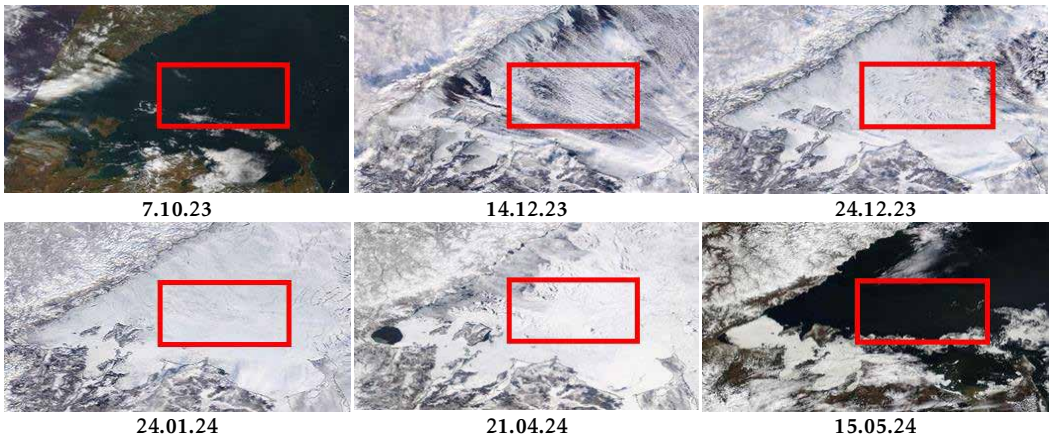

Figure 9. Images of the test site from MODIS data onboard the Aqua satellite with the study area boundary indicated by the red line.

After filtering, 4,736 points remained across 240 tracks for the period from September 2023 to August 2024. To quantitatively assess the evolution of the reflected signal DS shape for the Sea of Okhotsk test site, analogous statistical parameters were calculated. Figure 10 presents the dependencies of the Doppler spectrum maximum, width, and kurtosis on the measurement date. Similarly, block averaging was applied to the obtained dependencies.

Figure 10 shows that in the case of sea ice cover, a clear correlation between the values of statistical characteristics and the dates of ice cover growth is evident.

The obtained results indicate that freshwater ice cover exerts a significant influence on the statistical parameters of the Doppler spectrum. A dependence of peak power, DS width, and kurtosis coefficient on freshwater ice thickness was identified, which fundamentally distinguishes the properties of the signal reflected from freshwater ice from that reflected from sea ice.

In the case of sea ice, reflection occurs at the air–ice interface. First-year sea ice has high salinity ($\varepsilon \approx 4$–10 depending on salinity and temperature [*Shokr and Sinha*, 2015]), which results in a relatively high air–ice power reflection coefficient (0.11–0.27) and strong absorption within the brine-rich ice layer that prevents signal penetration to the ice–water interface. Therefore, the signal does not experience attenuation with varying ice thickness, and the DS width and kurtosis coefficient for sea ice remain stable regardless of thickness.

In contrast, for freshwater ice ($\varepsilon_{\text{ice}} \approx 3.2$ at L-band [*Mätzler*, 1998]), the air–ice power reflection coefficient is only about 0.08, meaning that most of the signal penetrates the ice layer. Reflection primarily occurs at the ice–water interface ($\varepsilon_{\text{water}} \approx 87$ at 0°C), where the

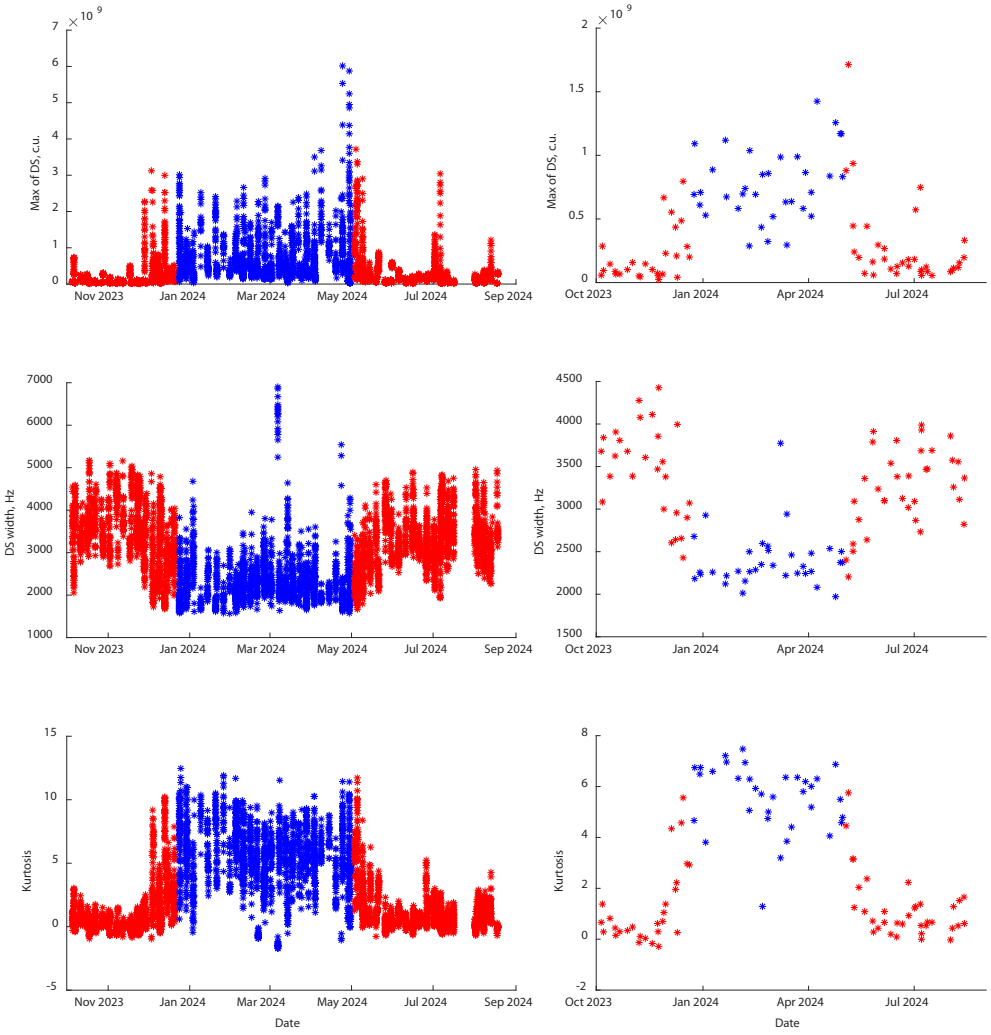

Figure 10. (a) From top to bottom: dependence of DS maximum, dependence of DS width, and dependence of kurtosis coefficient on date. (b) Same dependencies as in (a) after moving average smoothing.

reflection coefficient reaches approximately 0.46. Consequently, after complete ice cover formation and sustained negative air temperatures from January 4, 2024, the peak power began to decrease with increasing ice thickness, which is attributed to signal attenuation during propagation through the freshwater ice layer, as well as volume scattering from internal inhomogeneities. The Doppler spectrum width also decreased during the freezing period, indicating changes in geometric scattering conditions along with increasing absorption. During the spring melting period (April–May), the peak power remained nearly unchanged. These estimates are consistent with observations reported in [*Duguay et al.*, 2002; *Mätzler and Wegmüller*, 1987].

A number of limitations of the present study should be noted. ERA5 reanalysis data were used for ice cover thickness estimation rather than direct in situ measurements, which introduces additional uncertainty into the quantitative relationships between ice thickness and Doppler spectrum parameters. Furthermore, the spatial and temporal data coverage from the FY-3E satellite is determined by the random distribution of specular reflection points, which limits the uniformity of sampling. The study also did not consider the influence of snow cover, which may introduce additional signal attenuation and scattering, particularly under conditions of snow wetting during the spring period.

4. Conclusion

This study demonstrated, for the first time, the capability of spaceborne GNSS-R measurements at L-band for monitoring the full seasonal cycle of freshwater ice cover on a large inland water body. Using data from the GNOS-II instrument onboard the FY-3E satellite over Great Slave Lake (September 2023 – August 2024), it was shown that the statistical parameters of the Doppler spectrum – width and kurtosis coefficient – are sensitive to ice cover formation, growth, and break-up processes. A monotonic decrease in spectrum width with decreasing temperature was established, and a dependence of peak power and kurtosis on freshwater ice thickness was identified. Comparative analysis with sea ice in the Sea of Okhotsk revealed a fundamentally different behavior of the reflected signal, attributed to the difference in dominant reflection interfaces: the ice–water boundary for freshwater ice versus the air–ice boundary for saline sea ice.

The results suggest that GNSS-R Doppler spectrum analysis can serve as an effective tool for operational freshwater ice monitoring, complementing existing remote sensing methods with the advantages of L-band measurements: independence from cloud cover, illumination conditions, and weather. Future research will be directed toward validating the identified patterns on other freshwater water bodies using in situ ice thickness measurements, extending the analysis to multi-year time series to assess climate trends, and investigating the influence of snow cover on signal characteristics.

Acknowledgments. The study was supported by the Russian Science Foundation (grant No. 23-77-10064), https://rscf.ru/en/project/23-77-10064/.

References

Brown L. C. and Duguay C. R. The response and role of ice cover in lake-climate interactions // Progress in Physical Geography: Earth and Environment. — 2010. — Vol. 34, no. 5. — P. 671–704. — https://doi.org/10.1177/0309133310375653.

Duguay C. R., Bernier M., Gauthier Y., et al. Remote sensing of lake and river ice // Remote Sensing of the Cryosphere. — Chichester (UK) : Wiley, 2014. — P. 273–306. — https://doi.org/10.1002/9781118368909.ch12.

Duguay C. R. and Lafleur P. M. Determining depth and ice thickness of shallow sub-Arctic lakes using space-borne optical and SAR data // International Journal of Remote Sensing. — 2003. — Vol. 24, no. 3. — P. 475–489. — https://doi.org/10.1080/01431160304992.

Duguay C. R., Pultz T. J., Lafleur P. M., et al. RADARSAT backscatter characteristics of ice growing on shallow sub-Arctic lakes, Churchill, Manitoba, Canada // Hydrological Processes. — 2002. — Vol. 16, no. 8. — P. 1631–1644. — https://doi.org/10.1002/hyp.1026.

Gherboudj I., Bernier M. and Leconte R. A Backscatter Modeling for River Ice: Analysis and Numerical Results // IEEE Transactions on Geoscience and Remote Sensing. — 2010. — Vol. 48, no. 4. — P. 1788–1798. — https://doi.org/10.1109/tgrs.2009.2034256.

Hall D. K., Fagre D. B., Klasner F., et al. Analysis of ERS 1 synthetic aperture radar data of frozen lakes in northern Montana and implications for climate studies // Journal of Geophysical Research: Oceans. — 1994. — Vol. 99, no. C11. — P. 22473–22482. — https://doi.org/10.1029/94jc01391.

Hall D. K., Riggs G. A., Salomonson V. V., et al. MODIS snow-cover products // Remote Sensing of Environment. — 2002. — Vol. 83, no. 1/2. — P. 181–194. — https://doi.org/10.1016/s0034-4257(02)00095-0.

Howell S. E. L., Brown L. C., Kang K.-K., et al. Variability in ice phenology on Great Bear Lake and Great Slave Lake, Northwest Territories, Canada, from SeaWinds/QuikSCAT: 2000-2006 // Remote Sensing of Environment. — 2009. — Vol. 113, no. 4. — P. 816–834. — https://doi.org/10.1016/j.rse.2008.12.007.

Huang F., Xia J., Yin C., et al. Assessment of FY-3E GNOS-II GNSS-R Global Wind Product // IEEE Journal of Selected Topics in Applied Earth Observations and Remote Sensing. — 2022. — Vol. 15. — P. 7899–7912. — https://doi.org/10.1109/jstars.2022.3205331.

Jeffries M. O., Morris K., Weeks W. F., et al. Structural and stratigraphie features and ERS 1 synthetic aperture radar backscatter characteristics of ice growing on shallow lakes in NW Alaska, winter 1991-1992 // Journal of Geophysical Research: Oceans. — 1994. — Vol. 99, no. C11. — P. 22459–22471. — https://doi.org/10.1029/94jc01479.

Kang K.-K., Duguay C. R., Howell S. E. L., et al. Sensitivity of AMSR-E Brightness Temperatures to the Seasonal Evolution of Lake Ice Thickness // IEEE Geoscience and Remote Sensing Letters. — 2010. — Vol. 7, no. 4. — P. 751–755. — https://doi.org/10.1109/lgrs.2010.2044742.

Kang K.-K., Duguay C. R., Lemmetyinen J., et al. Estimation of ice thickness on large northern lakes from AMSR-E brightness temperature measurements // Remote Sensing of Environment. — 2014. — Vol. 150. — P. 1–19. — https://doi.org/10.1016/j.rse.2014.04.016.

Karaev V., Titchenko Y., Panfilova M., et al. On the Problem of the Sea Ice Detection by Orbital Microwave Doppler Radar at the Nadir Sounding // Remote Sensing. — 2022. — Vol. 14, no. 19. — P. 4937. — https://doi.org/10.3390/rs14194937.

Karaev V. Yu., Panfilova M. A., Titchenko Yu. A., et al. Monitoring of Inland Waters by Dual-Frequency Precipitation Radar: First Results // IEEE Journal of Selected Topics in Applied Earth Observations and Remote Sensing. — 2018. — Vol. 11, no. 11. — P. 4364–4372. — https://doi.org/10.1109/jstars.2018.2874697.

Karaev V. Yu., Sorokin E. S., Panfilova M. A., et al. On the Problem of Radar Monitoring of Ice Cover Formation and Destruction on Inland Waters: First Assessments // Russian Journal of Earth Sciences. — 2025. — Vol. 25. — ES3009. — https://doi.org/10.2205/2025es001020. — (In Russian).

Kouraev A. V., Semovski S. V., Shimaraev M. N., et al. Observations of Lake Baikal ice from satellite altimetry and radiometry // Remote Sensing of Environment. — 2007. — Vol. 108, no. 3. — P. 240–253. — https://doi.org/10.1016/j.rse.2006.11.010.

Kovaldov D. A., Karaev V. Y., Titchenko Y. A., et al. Reconstruction of the Angular Dependence of the Sea Ice Backscattering Pattern According to the GNSS-R Data // Russian Journal of Earth Sciences. — 2025. — No. 5. — ES5022. — https://doi.org/10.2205/2025es001082.

Kropáček J., Maussion F., Chen F., et al. Analysis of ice phenology of lakes on the Tibetan Plateau from MODIS data // The Cryosphere. — 2013. — Vol. 7, no. 1. — P. 287–301. — https://doi.org/10.5194/tc-7-287-2013.

Latifovic Rasim and Pouliot Darren. Analysis of climate change impacts on lake ice phenology in Canada using the historical satellite data record // Remote Sensing of Environment. — 2007. — Vol. 106, no. 4. — P. 492–507. — https://doi.org/10.1016/j.rse.2006.09.015.

Lehner B. and Doll P. Development and validation of a global database of lakes, reservoirs and wetlands // Journal of Hydrology. — 2004. — Vol. 296, no. 1–4. — P. 1–22. — https://doi.org/10.1016/j.jhydrol.2004.03.028.

Leigh S., Wang Z. and Clausi D. A. Automated Ice-Water Classification Using Dual Polarization SAR Satellite Imagery // IEEE Transactions on Geoscience and Remote Sensing. — 2014. — Vol. 52, no. 9. — P. 5529–5539. — https://doi.org/10.1109/tgrs.2013.2290231.

Long Z., Perrie W., Gyakum J., et al. Northern Lake Impacts on Local Seasonal Climate // Journal of Hydrometeorology. — 2007. — Vol. 8, no. 4. — P. 881–896. — https://doi.org/10.1175/jhm591.1.

Lopatin V. P., Murzabekov M. M. and Bobrov D. S. Results of determining the geoid height profile and vertical line deviation using GNSS signals reflected from water surface // Geodesy and Cartography. — 2024. — Vol. 1004, no. 2. — P. 21–30. — https://doi.org/10.22389/0016-7126-2024-1004-2-21-30. — (In Russian).

Mätzler C. Microwave Properties of Ice and Snow // Solar System Ices. — Dordrecht : Springer Netherlands, 1998. — P. 241–257. — https://doi.org/10.1007/978-94-011-5252-5_10.

Mätzler C. and Wegmüller U. Dielectric properties of freshwater ice at microwave frequencies // Journal of Physics D: Applied Physics. — 1987. — Vol. 20, no. 12. — P. 1623–1630. — https://doi.org/10.1088/0022-3727/20/12/013.

Mermoz S., Allain-Bailhache S., Bernier M., et al. Retrieval of River Ice Thickness From C-Band PolSAR Data // IEEE Transactions on Geoscience and Remote Sensing. — 2014. — Vol. 52, no. 6. — P. 3052–3062. — https://doi.org/10.1109/tgrs.2013.2269014.

Panfilova M. and Karaev V. Sea Ice Detection by an Unsupervised Method Using Ku- and Ka-Band Radar Data at Low Incidence Angles: First Results // Remote Sensing. — 2023. — Vol. 15, no. 14. — P. 3530. — https://doi.org/10.3390/rs15143530.

Panfilova M. and Karaev V. Sea Ice Detection Method Using the Dependence of the Radar Cross-Section on the Incidence Angle // Remote Sensing. — 2024. — Vol. 16, no. 5. — P. 859. — https://doi.org/10.3390/rs16050859.

Prowse T. D., Bonsal B. R., Duguay C. R., et al. River-ice break-up/freeze-up: a review of climatic drivers, historical trends and future predictions // Annals of Glaciology. — 2007. — Vol. 46. — P. 443–451. — https://doi.org/10.3189/172756407782871431.

Sharma S., Richardson D. C., Woolway R. I., et al. Loss of Ice Cover, Shifting Phenology, and More Extreme Events in Northern Hemisphere Lakes // Journal of Geophysical Research: Biogeosciences. — 2021. — Vol. 126, no. 10. — https://doi.org/10.1029/2021jg006348.

Shokr M. and Sinha N. K. Sea Ice: Physics and Remote Sensing. — Wiley, 2015. — (Geophysical Monograph Series). — https://doi.org/10.1002/9781119028000.

Titchenko Y. A., Karaev V. Y., Panfilova M. A., et al. Numerical Simulation of Radar Signal Reflected by Sea Surface with Different Sea Ice Concentration // Russian Journal of Earth Sciences. — 2025. — No. 3. — ES3007. — https://doi.org/10.2205/2025es001017. — (In Russian).

Weber F., Nixon D. and Hurley J. Semi-automated classification of river ice types on the Peace River using RADARSAT-1 synthetic aperture radar (SAR) imagery // Canadian Journal of Civil Engineering. — 2003. — Vol. 30, no. 1. — P. 11–27. — https://doi.org/10.1139/l02-073.

Yan Q. and Huang W. Spaceborne GNSS-R Sea Ice Detection Using Delay-Doppler Maps: First Results From the U.K. TechDemoSat-1 Mission // IEEE Journal of Selected Topics in Applied Earth Observations and Remote Sensing. — 2016. — Vol. 9, no. 10. — P. 4795–4801. — https://doi.org/10.1109/jstars.2016.2582690.

Yan Q. and Huang W. Sea Ice Sensing From GNSS-R Data Using Convolutional Neural Networks // IEEE Geoscience and Remote Sensing Letters. — 2018. — Vol. 15, no. 10. — P. 1510–1514. — https://doi.org/10.1109/lgrs.2018.2852143.

Yan Q., Huang W. and Moloney C. Neural Networks Based Sea Ice Detection and Concentration Retrieval From GNSS-R Delay-Doppler Maps // IEEE Journal of Selected Topics in Applied Earth Observations and Remote Sensing. — 2017. — Vol. 10, no. 8. — P. 3789–3798. — https://doi.org/10.1109/jstars.2017.2689009.

Yang Y., Moore P., Li Z., et al. Lake Level Change From Satellite Altimetry Over Seasonally Ice-Covered Lakes in the Mackenzie River Basin // IEEE Transactions on Geoscience and Remote Sensing. — 2021. — Vol. 59, no. 10. — P. 8143–8152. — https://doi.org/10.1109/tgrs.2020.3040853.

Zhu Y., Yu K., Zou J., et al. Sea Ice Detection Based on Differential Delay-Doppler Maps from UK TechDemoSat-1 // Sensors. — 2017. — Vol. 17, no. 7. — P. 1614. — https://doi.org/10.3390/s17071614.